Food Chemistry: X 15 (2022) 100407

Contents lists available at ScienceDirect

Food Chemistry: X

journal homepage: www.sciencedirect.com/journal/food-chemistry-x

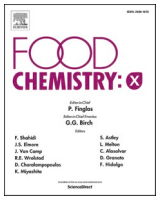

Aggregation of konjac glucomannan by ethanol under low-alkali treatment

Qinghui Song [a], Liangliang Wu [b], Shuhao Li [a], Guohua Zhao [a], Yongqiang Cheng [b], Yun Zhou [a,*]

[a] Chongqing Key Laboratory of Speciality Food Co-Built by Sichuan and Chongqing, College of Food Science, Southwest University, Chongqing 400715, China
[b] Beijing Key Laboratory of Functional Food from Plant Resources, College of Food Science and Nutritional Engineering, China Agricultural University, Beijing 100083, China

ARTICLE INFO

Keywords:
Konjac glucomannan
Ethanol
Low-alkali
Gelation
Aggregation

ABSTRACT

Utilizing ethanol in konjac glucomannan (KGM) gelation has important food processing applications. Typically, ethanol positively impacts the formation of low-alkali KGM gels and dramatically changes their physical properties, but the role of ethanol on the aggregation of KGM chains and the resultant gelation is less well understood. This study presents the distinct microstructures of low-alkali KGM gels incorporating ethanol. The fibril diameter and mesh size were determined to be 262.3 ± 22.3 nm and 2.680 ± 0.035 μm in average, contributing to a higher degree of anisotropy of such a gel network. Ethanol favors intermolecular aggregation by increasing the R_g of small-sized aggregates to 2.10 nm. The FTIR and temperature-cycled rheological studies suggest there are hydrophobic interactions stabilizing the gel network with the assistance of hydrogen bonds. The spatial confinement of deacetylated KGM chains as the solvent quality deteriorates by incorporating ethanol may arrange the aggregation and induce the structural reorganization in gel formation.

1. Introduction

Konjac glucomannan (KGM) known for the remarkable gel-forming capacity is a food hydrocolloid extracted from tubes of *Amorphophallus konjac* C. Koch, which has increasing worldwide popularity recently due to its physiological activities and health benefits (Devaraj, Reddy, & Xu, 2019). Chemically, KGM is composed of β-1,4-linked D-mannosyl and D-glucosyl residues at a molar ratio of (1.5 – 1.7): 1.0 with a small degree of β-1,3-branching linked at the C-3 position of mannose. Acetyl groups are essentially randomly distributed along the chain backbone with the degree of substitution around 0.05 – 0.11 (BeMiller, 2019). Heating KGM dispersions in the presence of alkalis or basic salts can form thermally irreversible heat-set gels. The understanding of KGM gelation has been evolving over the last decade and recently overviewed by Liu et al. (2021). Fundamentally, its gelation includes the deacetylation of KGM chain by alkali addition, the stretching and physically association of macromolecules upon heat-treatment, and the three-dimensional gel network established on the agglomeration of random network. In the structure of KGM there is a segregation into polar (OH groups) and nonpolar (CH groups) patches, and thus a clear amphiphilicity. For this reason, both hydrophobic interactions and hydrogen bonds are driving the aggregation of KGM and the resultant gel formation.

Despite a few experimental studies on gelation of concentrated KGM dispersions with no alkali addition (Jiang, Reddy, Huang, Chen, & Xu, 2019), it has been acknowledged that the strong alkaline environment is critical for gel-forming which only occurs at pH in the range of 11.3 – 12.6 (Huang et al., 2002). Depending on the alkali concentration, various important aspects of KGM gelation are expected to differ, such as the deacetylation and aggregation (Liu et al., 2021). It is a common practice to regulate the gelling rate and the mechanical strength of resultant gels by varying the alkali concentration (Solo-de-Zaldívar, Tovar, Borderías, & Herranz, 2014). Nevertheless, preparing KGM gels in the presence of such a considerable amount of alkaline also presents challenges associated with undesired product defects including significant syneresis, brown color and strong alkaline taste (Herranz et al, 2013), as well as a huge amount of alkaline wastewater produced subject to further treatment before its discharge. Developing alternative low-alkali or non-alkali KGM gelation is of practical importance and this is an active area of investigation currently.

In essence, the phenomenon of polysaccharide gelation arises from polymer chains being aggregated and entangled which can trap solvent via surface tension. It is clear that we can promote the gelation of polysaccharides, either by enhancing the aggregation or entanglement. Despite the noteworthy role of salt bridges, the tendency of the macromolecular chains to hydrate or aggregate is normally controlled and impacted by the balance between hydrogen bonds and hydrophobic

* Corresponding author at: College of Food Science, Southwest University, No. 2 Tiansheng Road, Chongqing 400715, China.
E-mail address: zhouy2017@swu.edu.cn (Y. Zhou).

https://doi.org/10.1016/j.fochx.2022.100407
Received 18 May 2022; Received in revised form 24 July 2022; Accepted 1 August 2022
Available online 4 August 2022

forces in aqueous environments (Ozbas, Kretsinger, Rajagopal, Schneider, & Pochan, 2004). Essentially, water molecules need to break some of their hydrogen bonds to accommodate macromolecules. This loss of hydrogen bonds between water and water will induce fluctuations and depletion of water density near large solutes. Therefore, hydrophobic interactions are originated from the collective motions of water hydrogen bond networks surrounding solutes (Jiang, Cao, Cheung, Zheng, Leung, Peng, & Huang, 2017). With regard to certain substances, sugars (*i.e.*, glucose, fructose and sucrose) and alcohols (*i.e.*, methanol, ethanol and glycerin) have manifested themselves as gelation promoters in various studies with underlying mechanism being explained by either the excluded volume effect which render those gelling polymers shrinking at low hydration levels or affecting the structural interactions: water molecules tend to be more restrained around those small molecules, promoting polymer–polymer interactions rather than polymer–solvent interactions. The gel of which the dispersing medium consists predominantly of an alcohol or a combination of alcohols and other solvent molecules is known as alcogel (Zhang, Song, Tian, Zhao, Zhou, 2022).

In an effort to reduce the alkali usage in KGM gel food processing, we have incorporated ethanol to facilitate the formation of KGM gels (Zhou et al., 2020). These scenarios addressed the extreme case of adding up to 40 vol% ethanol to the KGM dispersions with varying concentrations of alkali and provided convincing evidence for the discrepancies in the gel properties between those low-alkali or non-alkali KGM alcogels. It must be noted that the observed dissimilar nature of those KGM alcogels has not been elucidated yet in the absence of understanding of synergistic effect between the ethanol and alkali, which is fascinating not only out of scientific curiosity, but also for reducing alkali in konjac food processing.

In light of this, the present work was intended to address the specific role of ethanol on the given low-alkali KGM systems with regard to the structural interactions within KGM aggregation and the resultant KGM gelation. Rheological studies were performed to identify the macroscopic temperature- and time-dependent relaxation behaviors of each KGM system treated by either ethanol/alkali or both. The nanoscale gel structure was probed with some advanced *in situ* characterization techniques such as cryo-Scanning Electron Microscopy (cryo-SEM) and synchrotron-radiation Small-angle X-ray Scattering (SAXS) in conjunction with chemical structure study by Fourier Transform Infrared spectroscopy (FTIR). Before proceeding, it is worthwhile to know this study was not designed with a continuous change in ethanol and alkali concentrations, considering there had been research activity investigating the dose–effect relationship in KGM alcogels (Tong et al., 2022), while insight of structural features nevertheless was not satisfactorily explained in these studies.

2. Materials and methods

2.1. Materials

The purified konjac glucomannan (KGM) (>95.1 wt%, dry basis) was purchased from the Hubei Yizhi Konjac Biotechnology Co., ltd. (China). The contents of moisture and crude protein were 8.2 wt% and 0.76 wt%, respectively. The weight-average molecular weight of KGM was $2.59 \times 10^3 \pm 57.56$ kDa determined by gel permeation chromatography (GPC) using a dilute aqueous solution of KGM. All chemicals used were analytical grade and supplied by the Beijing Chemical Reagent Co., ltd. (China).

2.2. Sample preparation

The purified KGM was slowly dispersed in deionized water under magnetic stirring and swelled overnight at room temperature to obtain the 0.8 wt% KGM dispersion (denoted as K). The 0.04 wt% Na_2CO_3 and/or 20 % (v/w) ethanol were then added to KGM dispersions to prepare the dispersions of Na_2CO_3/KGM, ethanol/KGM and Na_2CO_3/ethanol/KGM abbreviated as AK, EK, and EAK, respectively. It should be noted that ethanol was added very slowly to the KGM dispersions upon agitating in order to prevent the pre-gel formation associated with localized rapid aggregation.

Structure characterizations, except the temperature sweep test, were employed on heat-treated K, AK, EK, and EAK. To clearly distinguish different states between samples, gels formed upon heating EK or EAK at 75 °C were denoted as EK_{gel} or EAK_{gel}, while K or AK with no gelling process observed even at 85 °C were denoted as K_{sol} or AK_{sol}.

2.3. Rheological measurements

The rheological behaviors of samples were measured with a DHR2 rheometer (TA Instruments, USA) with a Peltier plate temperature control system.

2.3.1. Temperature sweep test

The K, AK, EK, or EAK in their liquid state were loaded onto the bottom plate of the rheometer at 25 °C with a gap of 2 mm. The cycled temperature sweep at 0.5 % strain and 1 Hz were conducted by heating from 25 to 75 °C immediately followed by cooling down to 25 °C at a temperature scanning rate of 5 °C/min for three times. In this scenario, EK_{gel} and EAK_{gel} could be obtained *in situ* to make sure the EK and EAK in their gel state were intact before starting the temperature cycle. All the samples were over filling to minimize the impacts of evaporation due to continuous heating. Considering the huge difference in viscoelasticity between gels and sols, this setup was performed either under a 40 mm parallel plate (for EK and EAK) or 60 mm parallel plate (for K and AK). To prevent the slippery between wet gels and the geometry, axial force of 5 N was adopted with a sensitivity at 5 N.

2.3.2. Amplitude sweep test

The strain amplitude sweep measurements were conducted at a fixed frequency of 1 Hz with strains in the range from 0.1 % to 1000 %. The storage modulus G' and loss modulus G'' were recorded during measurements.

2.3.3. Creep-recovery test

The creep-recovery test was programmed in three intervals at constant 1 Hz with varying shearing stress: rest for 100 s at low shear stress of 10 Pa (the first interval) followed by structural deformation for 50 s at high stress of 50, 100, 150, 200, or 250 Pa (the second interval) and structural recovery for 100 s at low stress of 10 Pa (the third interval). A quantitative analysis of the structural deformation and recovery was made to represent the degree of structural deformation (D_{def}) and the degree of recovery (D_{rec}) of the hydrogels, which are expressed as below:

$$D_{def} = \left(G_1^{'} - G_2^{'}\right)/G_1^{'} \times 100\% \quad (1)$$

$$D_{rec} = \left(G_3^{'} - G_2^{'}\right)/G_1^{'} \times 100\% \quad (2)$$

where G_1' and G_2' are the last G' values of the first and the second interval, G_3' is the first G' value of the third interval.

2.4. Cryo-scanning electron microscopy (Cryo-SEM)

A small amount of sample (1 – 2 g) was placed into a slot on a stub with rivets and cryo-vitrified with liquid nitrogen rapidly to prevent the formation of large ice crystals. After being transferred onto a cryo-stage (at −160 °C) of the PP3010T Cryo-SEM Preparation System (Quorum Technologies, UK), samples were fractured and subsequently the frozen water was sublimated at −90 °C under controlled vacuum conditions. After 15 min, samples were sputtered with platinum using argon gas to prevent charging during electron beam targeting before being transferred on to the JSM 7100F SEM stage (JEOL ltd., Japan) at −160 °C and

scanned at a magnification of 1×10^4 (Patel et al., 2015).

All cryo-SEM images are segmented using Otsu thresholding by the open-source ImageJ software (National Institutes of Health, USA) in order to extract the network information. Removal of outliers was performed to remove noise and unwanted small objects from the structure. We segmented images using watershed by pixel flooding for pore partitioning and labelled those segmented meshes and watershed ridges for fibril diameter and mesh size calculation. Three images were used for each sample and ten different segments on each image were randomly measured.

2.5. Small-Angle X-ray scattering (SAXS) characterization

Synchrotron-radiation SAXS characterization was conducted at Synchrotron X-ray Beamline 1W2A in the Beijing Synchrotron Radiation Facility (BSRF, wavelength 0.154 Å). The wavelength was $\lambda = 1.54$ Å. The sample-to-detector distance was 2000 mm. EAK_{gel} and EK_{gel} were formed *in situ* in cuvettes by heating before measurements at room temperature. The background was determined by measuring the empty sample holder with solvents.

The FIT2D software (https://www.esrf.eu/computing/scientific/FIT2D/) was employed to transfer 2D scattering pattern to 1D scattering curve. The scattering vector was $q = 4\pi/\lambda \cdot \sin(\theta/2)$ and the θ is the scattering angle. Scattering curves can be used to differentiate between fractal dimensions which obey the power law: $I(q) \sim q^{-\alpha}$, where α is the slope of the straight line on a log–log plot scattering curves (Singhal, Toth, Beaucage, Lin, & Peterson, 1997). For mass fractals, one obtains $\alpha = D_f$ with $1 < D_f < 3$, and for surface fractals, $\alpha = 6 - D_f$ with $2 < D_f < 3$ (Gutsche, Guo, Dingenouts, & Nirschl, 2015).

2.6. Fourier transform infrared (FTIR) spectroscopy

FTIR spectra of freeze-dried K_{sol}, AK_{sol}, EK_{gel} and EAK_{gel} were assessed using an iS10 FTIR spectrometer (Nicolet, Germany) with a single reflection attenuated total reflectance (ATR) accessory equipped with a diamond crystal. The spectral range was 4000 – 400 cm^{-1} with a resolution of 4 cm^{-1}. All the spectra are an average of 200 scans with background and ATR correction.

2.7. Statistical analysis

The results are represented as mean ± standard deviation. Significant differences among the samples were determined by analysis of variance (ANOVA) and Duncan's test ($p < 0.05$), using the SPSS Statistics software (version 23.0, IBM Crop., USA).

3. Results and discussion

3.1. Temperature-dependence

The storage modulus (G') and loss modulus (G'') variation of K, AK, EK EAK with respect to a temperature cycle was plotted in Fig. 1. AK and K exhibited comparable mechanical response in terms of both heating and cooling (Fig. 1A). Albeit with a slightly higher G' than corresponding G'' upon cooling to 25 °C, AK and K were still in a sol state, which illustrate the role of the strong alkaline environment in gel-forming (Zhou et al., 2020). Even though the plotted data of EK exhibited some scatter when heating to beyond 55 °C, in part due to the gel syneresis and the ongoing ethanol evaporation as temperature raises. Opposite trends of moduli at elevated temperatures were observed in

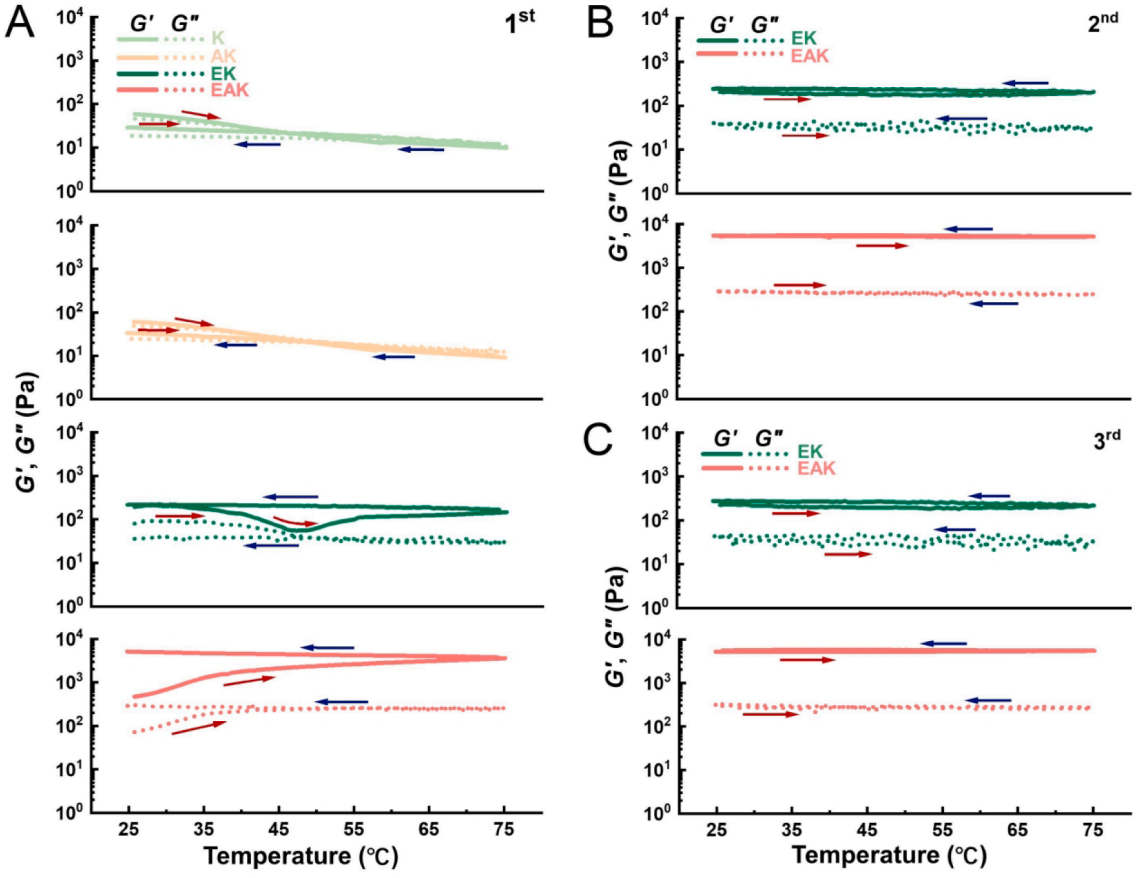

Fig. 1. Cycled temperature sweep of K, AK, EK and EAK: 1st (A), 2nd (B) and 3rd (C) temperature cycle. The red and blue arrows represent the heating and cooling process, respectively. (For interpretation of the references to color in this figure legend, the reader is referred to the web version of this article.)

EAK and EK (Fig. 1A). A closer examination of the temperature-dependence of G' revealed that EAK tended to be more elastic after heating, while EK experienced a G' slump before the recovery of elasticity during the latter heating processing, similar to what happened in the induction of KGM gelation in the presence of alkali (Williams, Foster, Martin, Norton, Yoshimura, & Nishinari, 2000). The representative gelation of KGM upon alkali-treatment has been illustrated by Liu et al. (2021), which could at least give some clues on the structural changes behind this trend of G'. However, it is still interesting to know the impacts of ethanol on KGM gelation can be altered at such a low alkali concentration.

Despite the post-gelation behavior of KGM gel being long ignored for simplicity and discussed only in limited studies, usually in conjunction with the significant syneresis effect (Herranz et al, 2013), the G' and G'' of EAK did not vary during the cooling and no hysteresis in the moduli between the heating and cooling curves was observed in both the second and the third temperature cycles. However, hysteresis always existed for EK in several temperature scans (Fig. 1B and 1C). From purely a thermodynamics perspective, the hysteresis could be driven by the changes in the role of the entropic term of water and macromolecule-solvent interactions, which could be reflected on the changes in hydrogen bonding (Wang, Liu, Ru, Bai, & Feng, 2016). Regardless of the thermodynamics, the resistance of gel to temperature changes could be ascribed to a structural explanation as well. In essence, time and temperature are equivalent in terms of relaxation and the physical associations are expected to be transient which will relax on a timescale comparable to the lifetime of the given physical associations (Dooling, Buck, Zhang, & Tirrell, 2016). When the given heating condition was applied, there was sufficient time for EK to relax, while it was not enough for EAK to do so. Thus, we presumed there were some interactions or structural components which would stabilize the network even when the physical associations were largely weakened upon heating.

3.2. Deformation-recovery behaviors

We investigated the solid–liquid transition of EAK_{gel} and EK_{gel} by measuring the dynamic moduli under strain amplitude increment. Both gels could sustain finite deformations, which could quickly recover by releasing external forces on the timescale of the experiment before approaching the linear viscoelastic strain limits (*i.e.*, 49.8 Pa for EAK_{gel} and 2.3 Pa for EK_{gel}), if strain was converted to stress (Fig. 2A). Such a stress value probably reflected the elastic strength of the interactions between neighboring structural elements. The primary breakup of the soft semi-solid structure is actually a small-scale phenomenon which normally occurs at the scale of an individual structural element such as the stiffness of the elastic bonds, and is insensitive to the coupling between neighboring structural units, *i.e.*, interconnection by fairly weak hydrogen bonds (Andreas, PutzTeodor, & Burghelea, 2009). However, the subsequent loss of solidity corresponds to the interactions between structural units in a larger spatial scale and obviously, such a structural unit of EAK_{gel}, albeit not well-defined yet, was supposed to be superior in rigidity in comparison with EK_{gel}, given much higher values of G' for EAK_{gel}.

When local deformations exceeded such certain linear strain limits, elastic-solid nature of the gel began to change and stepped into the

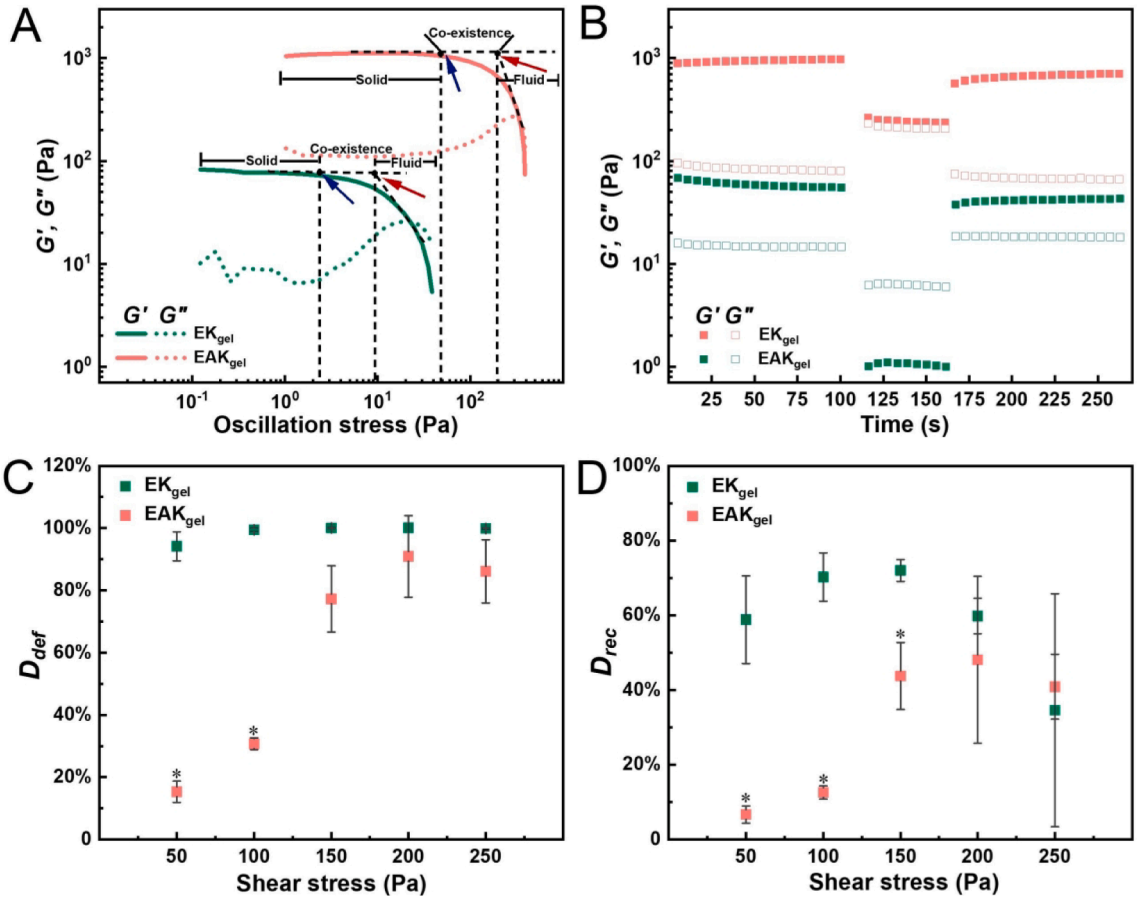

Fig. 2. Mechanical response as a function of oscillation shear stress (A) and to a three-interval thixotropic test at interval stress of 50 Pa for EK_{gel} or 250 Pa for EAK_{gel} (B); degree of deformation (C) and degree of recovery (D) calculated based on the three-interval thixotropic tests at varying interval stresses. The blue and red arrows indicate the end of linear viscoelastic region and the yield point, respectively. Asterisk (*) indicates significant difference at the same shear stress ($P < 0.05$). (For interpretation of the references to color in this figure legend, the reader is referred to the web version of this article.)

solid–fluid phase co-existence regime (Hamada, Gakhar, & Longo, 2021). There was a competition between the destruction and reformation of the gel. The break-up of the gel network is commonly accepted to be the microscopic scale origin of the macroscopic yielding. Applied external forces could definitely cause a damage to the structural units, but such a force was not large enough to allow entire recombination in a different configuration and part of them could have enough time to recover subject to slow deformation (Ju, Ha, Song, & Lee, 2021). Thus, this preyielding process could be attributed to the heterogeneity of the gel network. A broader spectrum of phase co-existence might result from a higher level of spatial heterogeneity (Andreas, PutzTeodor, & Burghelea, 2009).

More spectacular differences, however, were observed when comparing the nonlinear response of EK_{gel} to that of EAK_{gel}. The co-existence regimes ended at 8.869 Pa and 173.014 Pa for EK_{gel} and EAK_{gel}, depicted by red arrows in Fig. 2A. This critical stress, which is typically obtained from the intersection of two asymptotic lines drawn through the initial and post-breakdown modulus data, can be considered to be an approximate measure of the yield stress of the material (Rafe, & Razavi, 2013). EK_{gel} and EAK_{gel} were subject to viscous flow at the macroscopic level in the nonlinear region, where entire interactions between neighboring structural units were broken and the probability of their rebinding was negligibly small. As a consequence, the destruction of the gel network prevailed in the viscous flow regime. However, there was a visible peak on their G'' curves in this purely viscous regime revealing strain amplitude where energy dissipation was maximized, which was assigned to the weak strain overshoot archetype. The underlying origins of overshoot were thought to be a variation of microstructure, either compacting of clusters that pushed the gel system towards phase separation or restructuring of clusters which would ultimately rupture in individual pieces. Compared to EK_{gel}, the overshoot was largely magnified in EAK_{gel}, probably because larger and better-defined clusters was formed in the sheared EAK_{gel} network at different shear stress (Wagner, & Mewis, 2021).

To further identify the difference of stress response and recovery behaviors between EAK_{gel} and EK_{gel}, we implemented several stress-varying interval thixotropic tests that includes both deformation and recovery processes. Considering EAK_{gel} and EK_{gel} did not share the same viscous flow regimes, we selected 250 Pa and 50 Pa for EAK_{gel} and EK_{gel} as the corresponding applied stress for breaking the structural unites and hence we can observe their deformation and recovery behaviors (Fig. 2B). As already pointed out, due to the strong heterogeneity of the gel network, the break-up and reconstruction of these structural unites should, in principle, occur over a whole interval of applied stresses (Andreas, PutzTeodor, & Burghelea, 2009).

The observed decrease of G' shown in Fig. 2B was accompanying with the implementation of the second interval and G' was found to be very close or even much smaller to G'' during deformation, indicating that EK_{gel} and EAK_{gel} were already in a fluid state due to a structural break-up (Shitrit, & Bianco-Peled, 2021). However, they presented quite different flow behaviors. In terms of EK_{gel}, G' is nearly negligible (≈ 1 Pa), once again confirming its purely viscous nature. In contrast, the comparable G'' to G' of EAK_{gel} implied an anomaly with the assumption that microscopic environment of broken network is not primarily viscous. It is more plausible to consider it is a viscous environment consist of concentrated centers of strongly associated macromolecules surrounded by regions of dilute macromolecular solution. The underlying origins of the difference were thought to be either structural or conditional. Therefore, we conducted a quantitative analysis of the structural deformation and recovery by applying several stresses over a broad spectrum and results were represented in Fig. 2C and 2D.

Both the degree of deformation (D_{def}) and the degree of recovery (D_{rec}) of EAK_{gel} were much less than the EK_{gel} ($P < 0.05$) in operating stress conditions < 100 Pa, thus revealing the structural origin of the phenomenon. We also noted anywhere from 150 to 250 Pa to applied shear stress beyond 250 Pa, the deformation-recovery behaviors of each gel were rather not significantly different. Namely, gel structure did not make a difference in the deformation-recovery behaviors and instead the external force dominated the structural transition given very high applied stress. Significant deviations in the D_{def} and D_{rec} of EAK_{gel} occurring compared to EK_{gel}, which is especially apparent at higher shear stress, could be explained by the restructured gel morphology with more anisotropy and a less well-defined structural patterns (Ju, Ha, Song, & Lee, 2021).

3.3. Gel microstructure

We employed direct imaging to provide some insights into the microstructure patterns with cryo-SEM, which could overcome the shortcoming of dehydration which might cause the severe collapse and flattening. Typical cryo-SEM images for EK_{gel} and EAK_{gel} were shown in Fig. 3A.

Overall, both gels were essentially composed of highly interconnected network structures where the water was embedded in both the large pores and small meshes. We could see those networks were inserted with some locally flat walls probably caused by the artificial reorganization such as frozen fracture and drying orientation (Wu, Gaharwar, Chan, & Schmidt, 2011). The cryo-SEM images of K_{sol} and AK_{sol} could be also found in Fig. S1, presenting morphological pictures of KGM dispersion in polar solvent due to the strong role of KGM/solvent interactions. On macroscopic level, the freeze-drying process allows for the achievement of monoliths that preserve the size and shape of the container submitted to freezing. In colloid dispersions, spaces originally resided by ice crystals are transformed to empty areas enclosed by "walls" of matter, leading to ordered porous structures rather than interconnected networks, while such an oriented honeycomb-like structure may be formed in the sublimation of icy crystals (Tripathi, Parsons, Khan, & Rojas, 2018). As a result, KGM chains were mostly aggregated and sequestered into unfrozen water regions, thus being contained in the dense wall-like structures.

A visual inspection of Fig. 3A revealed that EAK_{gel} were relatively disordered in network configuration, while the network of EK_{gel} displayed a lower degree of anisotropy. This result was consistent with aforementioned a broader spectrum of solid–fluid co-existence for EAK_{gel}. The structure of fibril, as one of the integral components of morphological investigations on gel network, was illustrated by presenting its diameter distribution in Fig. 3B. When the fibril diameter data were plotted together, there is a significant deviation between the mean, median (*i.e.*, D50) and mode diameters (Table S1), existing in a non-symmetric distribution, reflecting the dimensional anisotropy of fibrils as a natural consequence of the complex multiscale aggregation of KGM chains in the whole scanned regime.

EAK_{gel} appeared to be not significantly different with EK_{gel} in terms of mode and D50 values, but the average diameters of those rod-like elongated aggregated fibril, determined to be 193.8 ± 34.1 nm and 262.3 ± 22.3 nm for EK_{gel} and EAK_{gel}, were significantly increased with alkali. The distinction in diameter of fibril was in accord with the visual inspection of gel network in Fig. 3A and revealed the tendency of agglomeration of fibrils in EAK_{gel}. In principle, the size of the fibril is determined by the elastic energy required to form the rod-like structure aggregated from macromolecules, and the interfacial energy associated with the macromolecule-solvent interactions that tends to decrease by minimizing the surface area. The aggregated supramolecular nanodomains of EAK_{gel} which could agglomerate into larger and stronger rod-like aggregates and further hierarchical network structures could probably be the individual structural element contributing to the elastic strength discussed above. The resultant thicker fibrils were much stronger, and hence provided stiffness to the network. In light of recent evidence providing that both EAK_{gel} and EK_{gel} are composed of a semi-crystalline KGM matrix (Fig. S2), although the crystalline structure is not definitively known, those nanodomains were illustrated to be a certain low degree of crystallinity, but packed differently under different

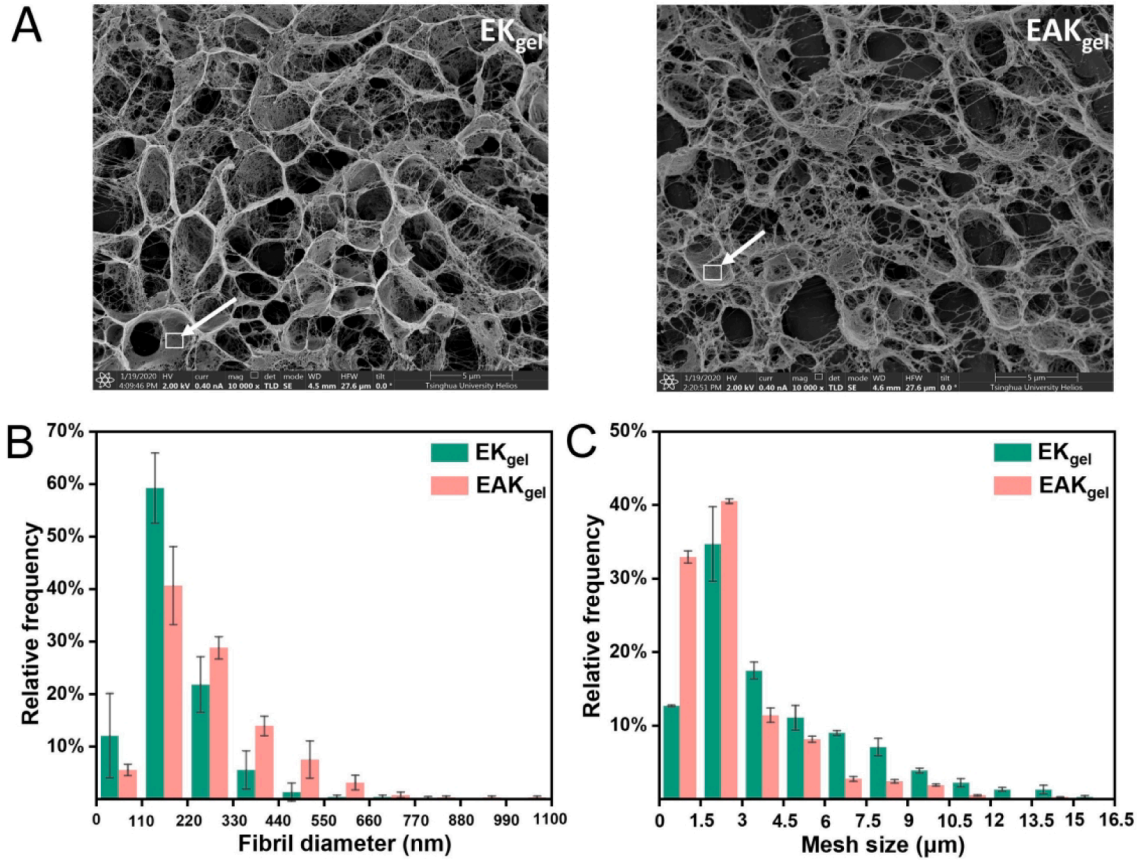

Fig. 3. Typical cryo-SEM images of EK_{gel} and EAK_{gel} (A) and morphological descriptions based on the quantative analysis of the direct imaging from cryo-SEM: distribution of diameter of fibril (B) and mesh size (C). White arrows represent the locally flat walls.

conditions.

The network of EAK_{gel} seemed to be denser than that of EK_{gel} shown in Fig. 3A. However, the highly anisotropic characteristics of gel network made representation of morphology with an accurately quantification of domains, shape, distribution, and connectivity, especially across meshes really challenging. Thus, we tried segmenting cryo-SEM images using Otsu thresholding, whereby we were able to recognize the differences in the network displayed in Fig. 3A. As shown in Fig. 3C, a shift of mesh size distribution and size toward smaller range was seen in EAK_{gel} (see also Table S2). While the small hydrophobic mesh enabled a continuous transport pathway of external force through the network, its mechanical stability could be improved as illustrated in Fig. 2C. Moreover, smaller mesh could also be interpreted as there is the smaller spacing between the physically associated zone. By combining with the rheological study results, we could expect the physically associated zone was much stronger for EAK_{gel}, and hence provided stiffness to the network. Albeit with systematic artificial reorganization, the smaller spacing between association zones implied the existence of the synergistic effect of ethanol and alkali (Tong et al., 2022), even at very low concentration. Introducing ethanol can prolong the interaction time between two colliding aggregates, which fluctuated by thermal motion. If the interaction time is much longer than the time required for macromolecular aggregates to diffuse, penetrate and merge, the probability of fusing into large associated zone can be largely increased. Herein, it is more conducive to the formation of smaller spacing between association in the case of alkali treatment which can induce deacetylation and eliminate such internal constraints against fusing (unpublished data). Thus, it is important to gain insights into the characteristic structure of those association zone.

3.4. Characterization of KGM aggregates

Fig. S3 displays the SAXS spectra with the corresponding length scale. The q is proportional to the inverse of the apparent periodic length d, as $d = 2\pi/q$ (Wang et al., 2018). The scale of length was determined to be ~ 6 nm, confirming the extracted SAXS data was scattering of KGM aggregates or the interior substructures of aggregates. Typically, there are two commonly studied q-regimes: the small-q upturn Guinier regime providing information about larger-scale structural features of scatterer and the large-q Porod regime providing information about the interface of scatterer (Gutsche, Guo, Dingenouts, & Nirschl, 2015).

In Fig. S3, SAXS profiles manifest themselves in the asymptotic regime of Porod as there was a strong continuous decrease in scattering intensity with a characteristic slope. As we can see from the logarithmic plots, which were no longer straight lines, the assemblage should contain a distribution of aggregate size. The average physical quantity related to the spatial distribution of the mass, *i.e.*, radius of gyration (R_g) was measured for aggregate size interpretation. To determine the R_g of each aggregate fraction of each sample, graphical reduction was employed with results being showed in Table 1 (see Fig. S4 and Table S3 for the complete calculation by the method of graphical reduction).

We found the R_g of K_{sol} was significantly smaller than others in Table 1 and both the large and middle-sized aggregates were negligible in volume fraction for K_{sol}. Giving the nearly monodisperse nature of KGM aggregates of K_{sol} at nanoscale, K_{sol} formed a colloid system with very small aggregates of KGM since the macromolecule backbones tend to be stretching without any treatments. In terms of the alkali or ethanol treated sample, the KGM aggregates were as expected to differ in size (Table 1). Deacetylated KGM molecules did not stretch but rater exhibited dispersion-like behavior with spherical aggregates (Zhou et al., 2018). It has been well accepted that the deacetylation

Table 1
The radius of gyration (R_g) of KGM aggregates with its corresponding weight fraction acquire from cascade tangent rule.

KGM aggregates	R_g (nm)	Weight fraction	D_f
K_{sol}	0.85	99.89 %	1.780
	2.25	0.09 %	
	3.21	0.02 %	
AK_{sol}	1.31	99.36 %	2.180
	1.75	0.53 %	
	3.00	0.11 %	
EK_{gel}	1.17	98.63 %	2.278
	1.25	1.30 %	
	3.70	0.07 %	
EAK_{gel}	2.10	99.63 %	2.874
	3.33	0.23 %	
	3.77	0.13 %	

significantly reduces the steric hindrance (Qiao et al., 2022), which will favor intermolecular aggregation. And it was observed such a low concentration of alkali could remove almost all the acetyl groups along the KGM chain (~95 % degree of deacetylation for EAK_{gel} and AK_{sol}).

Surprisingly, despite the gel nature of EK_{gel}, its KGM aggregates were even smaller than AK_{sol} in the spatial distribution of the mass. It is seemingly difficult to imagine that such a collapsed aggregate structure could overcome the rotation agitated by thermal energy, making the chains confined within entanglements, unless the surrounding solvent deteriorated in quality and inhibited the slippery because of the more negative excluded volume effect. KGM aggregates of EAK_{gel} were relatively the largest, suggesting only with both alkali and ethanol did these aggregating effects coming come into play. The size of the aggregates is determined by the elastic energy required to form the rod-like structure, the interfacial energy that tends to decrease by minimizing the surface area, and most importantly, the spatial confinement effect associated with the KGM – solvent interactions. The small-sized KGM aggregates of AK_{sol} and EAK_{gel} was very similar in weight fraction (99.36 % vs 99.63 %). Suppose the deacetylation was completed much faster than the intermolecular aggregation, we could propose the associated zones of EAK_{gel} were not distributed in the polymer network, but only located at the original junction zones of alkali gels essentially composed of acetyl-free portions. In addition to the (main) correlation region, there is two sharp peaks (see Fig. S3) in the EAK_{gel} spectra indicated by arrows, clearly revealing KGM molecules could assembled into some small-scale ordered structures (Wang et al., 2018), *i.e.*, the nanodomains aforementioned. Nevertheless, there is no peak exhibiting in curves other than EAK_{gel}, suggesting that the KGM aggregates are mostly homogenous and amorphous on the length scale of this experiment.

As the interior structure of aggregates is expected to consist of a complex "fractal-like" micropores, the values of D_f (see Table 1) were also extracted by scaling $I(q)$ in the asymptotic regime of Fig. S3, those were 1.78, 2.18, 2.278 and 2.874 for K_{sol}, AK_{sol}, EK_{gel} and EAK_{gel}. We obtained mass fractal with $1 < D_f < 3$, which has been positively related to the compactness of the scatterer (Shilova, 2020) and thus the free volume in the scatterer can be interpreted, *i.e.*, larger mass fractal indicates smaller volume of the micropore. The closely spaced hydroxyls in the hydrogen-bonded form would endow aggregates substructures with more continuous and better-connected domains. Otherwise, KGM aggregates could be loosened due to the larger volume of such micropores which can accommodate water clusters. Key to that assumption is the local environment of hydrogen bonds and their property, which has been probed by FTIR.

3.5. Hydrogen bonding

We attended to interpret the aggregation of the KGM backbone via the with a focus on the analysis of the IR information related to hydrogen bonding induced changes in hydroxyl-water local environment (see Fig. 4). The characteristic IR fingerprints of KGM are associated with the

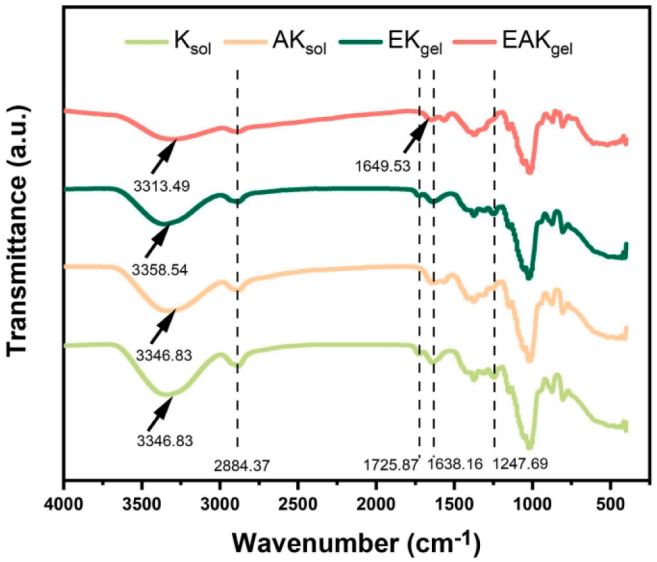

Fig. 4. FTIR spectra of K_{sol}, AK_{sol}, EK_{gel} and EAK_{gel}.

macromolecular chains (the stretching bands for $-CH_2$ and C—O at 2884 cm^{-1} and 1247 cm^{-1}), acetyl groups (asymmetric ν_{as}(C═O) at 1725 cm^{-1}) and interacting with free water (H—O—H bending at 1620 – 1740 cm^{-1}, ν(O—H) stretching at 3000 – 3450 cm^{-1}, and 1638 cm^{-1} for hydroxyl groups associated of C—O (Ye, Kennedy, Li, & Xie, 2006). The peak at 1725 cm^{-1} for both AK_{sol} and EAK_{gel} disappeared in the spectra, indicating that all the acetyl groups had been removed as a result of alkali treatment.

The absorption bands at 1638 cm^{-1} and 3000 – 3500 cm^{-1} being assigned to ν(O—H) stretching could be used to identify the in-plane deformation of the water molecule and local hydrogen bonding environment (Wu et al., 2012). As noted, the latter characteristic absorption band was wide and strong in each IR spectra, demonstrating the existence of hydrogen bonded hydroxyls and thus the shifts in this band are ascribed to alternations in the extent of the formation of intra-or intermolecular hydrogen bonding (Wang et al., 2020). Despite the ν(O—H) band at 3000 – 3500 $cm^{-1}$of EAK_{gel} being down-shifted to 3313.49 cm^{-1}, the band at 1638 cm^{-1} up-shifted to 1649 cm^{-1}, suggesting the hydrogen bonding stack size has been changed (Panja, Dietrich, Trabold, Zydel, Qadir, & Adams, 2021), which probably lead to different molecular packing in the EAK_{gel}. What occurred in EAK_{gel} IR spectra could be interpreted as the existence of the chains with largely restricted motion in confined spaces. Albeit with the tendency for such a stretched macromolecular chain in EAK_{gel} to contract to increase its conformational entropy, as thermodynamics reveals an isolated system always spontaneously moves towards the direction of increasing entropy (Fang, 2021), it is critical to understand why this happens only in EAK_{gel} and that is, only segments of deacetylated KGM chain with ethanol-treatment randomly move inside a 'smaller box' indicated by the SAXS analysis and can still approach the neighbor chains for hydrogen bonding.

In principle, the chain motion has opposite dependence on excluded volume and entropy elasticity effects and their competition allows each macromolecular chain to approach or repel each other (Kreer, 2016). It is reasonable to understand ethanol can change the balance of this competition by increasing the translational entropy and excluded volume will limit the motion of chain. The hydrophobic interaction thus plays a pivotal role in controlling the molecular packing in the gelation of EAK_{gel}, instead of hydrogen bonding. However, the extent of contributions from hydrophobicity to this process still remains unclear because quantitative measurements of hydrophobic interactions are very challenging.

When it comes to the impact of alkali, the distinct conformations of

deacetylated KGM chain in a comparison with the native one, which were evident from the study of Zhou et al (2018), could explain the intrinsic factors controlling the entropy elasticity effects, if we treated the KGM chain as a spring with similar length even after the removal of acetyl. Unequivocally, impact of ions on excluded volume of neutral KGM chains is expected to be negligible in a comparison with that of ethanol. Besides the apparent R_g of KGM aggregates, the differences in properties of the EKgel and EAKgel can be also ascribed to the change in underlying molecular packing due to the existence of different non-covalent interactions.

3.6. Aggregation of KGM by ethanol under low-alkali treatment

Combining, several features of ethanol and low-alkali treated KGM aggregation could be outlined from the provided data on EAK_{gel} as shown in Fig. 5: a) intermolecular aggregation of KGM chains was intensified; b) patterns exhibited stronger anisotropy in gel network; c) KGM fibrils were possibly formed with some random small-scale ordered nanodomains inserted in; d) there might be preferential hydrophobic interaction than hydrogen bonding constraining the associative domain.

Similar to the gelation of pectin, alginate, xanthan and guar gum, there was an increase of solvent hydrophobicity due to addition of ethanol (Tkalec, Knez, & Novak, 2015). Consistent with observations reported in the literature, the formation of some nanodomains could lead to spatial segregation of KGM aggregates, which would concentrate in the diminishing water domains as the alcohol content increases and the extent of the aggregation would be tied to the ability of the alcohol to create these nanodomains (da Silva, Calabrese, Schmitt, Celebi, Scott, & Edler, 2018). The self-association of cellulose in alcoholic aqueous binary mixtures which leads to the occurrence of inhomogeneous clustering at short length scales has been reported (From, Larsson, Andreasson, Medronho, Svanedal, Edlund, & Norgren, 2020). Studies of cellulose derivatives also pointed to the strong effect of short-lived hydrophobic interactions in aqueous solution, but there is no indication of hydrogen bonding driving association between the cellulose derivatives molecules in water or playing a role in association phenomena in general (Lindman, Medronho, Alves, Costa, Edlund, & Norgren, 2017). Notably, this indicates that low-alkali treatment will affect the KGM aggregation and ethanol cannot be considered as the only influencing factor.

4. Conclusion

Recent developments on KGM alcogels has provided significant improvements on reducing the alkali usage in konjac food processing. A related issue that is garnering much more attention is why KGM can gel under a low-alkali condition in an ethanol-containing solvent system. In view of the discrepancy in multiscale structure between K_{sol}, AK_{sol}, EK_{gel} and EAK_{gel}, ethanol could intensify the intermolecular aggregation of KGM chains and created stronger anisotropy in gel network with some random nanodomains of deacetylated KGM aggregates. The existence of different molecular packing patterns between the EKgel and EAKgel could be interpreted as a result of different non-covalent interactions holding KGM chain in a spatial confined configuration. Inspired by these observations, we propose the arranged structural reorganization in EAK_{gel} could be attributed to the aggregation of deacetylated KGM chains as the solvent quality deteriorates. Such systems serve as proxies for complex intermolecular association in the gelation of carbohydrate polymers under ethanol and exhibit phenomena associated with excluded volume effect and related hydrophobic interaction.

CRediT authorship contribution statement

Qinghui Song: Methodology, Validation, Formal analysis, Investigation, Data curation, Writing – original draft, Visualization. **Liangliang Wu:** Methodology, Formal analysis, Investigation, Data curation. **Shuhao Li:** Software, Visualization. **Guohua Zhao:** Project administration. **Yongqiang Cheng:** Supervision, Project administration, Funding acquisition. **Yun Zhou:** Conceptualization, Project administration, Supervision, Writing – original draft, Writing – review & editing.

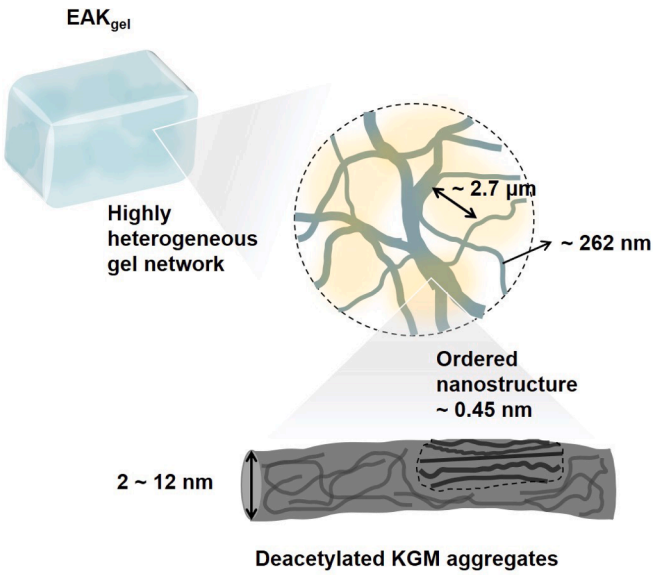

Fig. 5. Illustration of the multiscale structure of EAK_{gel}.

Declaration of Competing Interest

The authors declare that they have no known competing financial interests or personal relationships that could have appeared to influence the work reported in this paper.

Acknowledgements

This work was supported by Natural Science Foundation of Chongqing (cstc2021jcyjmsxmX0025), Fundamental Research Funds for the Central Universities (XDJK2020C051), Postgraduate Mentor Team-building Program of Southwest University (XYDS201905), Technology Innovation and Application Development Special Funds of Chongqing (cstc2019jscx-dxwtBX0031 & cstccstc2021jscx-tpyzxX0019) and the grant from Development and Research Center of Sichuan Cuisine (CC21Z13). The authors thank 1W2A SAXS station at the Beijing Synchrotron Radiation Facility (BSRF) for courteously supporting the SAXS analysis.

Appendix A. Supplementary data

Supplementary data to this article can be found online at https://doi.org/10.1016/j.fochx.2022.100407.

References

Andreas, M. V., PutzTeodor, I., & Burghelea. (2009). The solid–fluid transition in a yield stress shear thinning physical gel. *Rheologica Acta, 48*, 673–689. https://doi.org/10.1007/s00397-009-0365-9

BeMiller, J. N. (2019). Inulin and konjac glucomannan. *Carbohydrate Chemistry for Food Scientists*, 253–259. https://doi.org/10.1016/b978-0-12-812069-9.00010-8

da Silva, M. A., Calabrese, V., Schmitt, J., Celebi, D., Scott, J. L., & Edler, K. J. (2018). Alcohol induced gelation of TEMPO-oxidized cellulose nanofibril dispersions. *Soft Matter, 14*(45), 9243–9249. https://doi.org/10.1039/C8SM01815D

Devaraj, R. D., Reddy, C. K., & Xu, B. J. (2019). Health-promoting effects of konjac glucomannan and its practical applications: A critical review. *International Journal of Biological Macromolecules, 126*, 273–281. https://doi.org/10.1016/j.ijbiomac.2018.12.203

Dooling, L. J., Buck, M. E., Zhang, W. B., & Tirrell, D. A. (2016). Programming molecular association and viscoelastic behavior in protein networks. *Advanced Materials, 28*(23), 4651–4657. https://doi.org/10.1002/adma.201506216

Kreer, T. (2016). Polymer-brush lubrication: A review of recent theoretical advances. *Soft Matter, 12*(15), 3479–3501. https://doi.org/10.1039/C5SM02919H

Fang, Y. (2021). Mixed hydrocolloid systems. *Handbook of Hydrocolloids (Third Edition)*, 125–155. https://doi.org/10.1016/B978-0-12-820104-6.00018-8

From, M., Larsson, P. T., Andreasson, B., Medronho, B., Svanedal, I., Edlund, H., & Norgren, M. (2020). Tuning the properties of regenerated cellulose: Effects of polarity and water solubility of the coagulation medium. *Carbohydrate Polymers, 236*, Article 116068. https://doi.org/10.1016/j.carbpol.2020.116068

Gutsche, A., Guo, X., Dingenouts, N., & Nirschl, H. (2015). Synthesis and small angle X-ray scattering (SAXS) characterization of silica spheres covered with gel-like particles formed by means of solvent evaporation. *Powder Technology, 278*, 257–265. https://doi.org/10.1016/j.powtec.2015.03.037

Hamada, N., Gakhar, S., & Longo, M. L. (2021). Hybrid lipid/block copolymer vesicles display broad phase coexistence region. *BBA - Biomembranes, 1863*(4), Article 183552. https://doi.org/10.1016/j.bbamem.2021.183552

Herranz, B., Tovar, C. A., Solo-de-Zaldívar, B., & Borderias, A. J. (2013). Influence of alkali and temperature on glucomannan gels at high concentration. *LWT - Food Science and Technology, 51*(2), 500–506. https://doi.org/10.1016/j.lwt.2012.11.023

Huang, L., Takahashi, R., Kobayashi, S., Kawase, T., & Nishinari, K. (2002). Gelation behavior of native and acetylated konjac glucomannan. *Biomacromolecules, 3*(6), 1296–1303. https://doi.org/10.1021/bm0255995

Jiang, L., Cao, S., Cheung, P. P. H., Zheng, X., Leung, C. W. T., Peng, Q., & Huang, X. (2017). Real-time monitoring of hydrophobic aggregation reveals a critical role of cooperativity in hydrophobic effect. *Nature Communications, 8*(1), 1–8. https://doi.org/10.1038/ncomms15639

Jiang, Y., Reddy, C. K., Huang, K., Chen, L., & Xu, B. (2019). Hydrocolloidal properties of flaxseed gum/konjac glucomannan compound gel. *International Journal of Biological Macromolecules, 133*, 1156–1163. https://doi.org/10.1016/j.ijbiomac.2019.04.187

Ju, Y., Ha, J., Song, Y., & Lee, D. (2021). Revealing the enhanced structural recovery and gelation mechanisms of cation-induced cellulose nanofibrils composite hydrogels. *Carbohydrate Polymers, 272*, Article 118515. https://doi.org/10.1016/j.carbpol.2021.118515

Lindman, B., Medronho, B., Alves, L., Costa, C., Edlund, H., & Norgren, M. (2017). The relevance of structural features of cellulose and its interactions to dissolution, regeneration, gelation and plasticization phenomena. *Physical Chemistry Chemical Physics, 19*(35), 23704–23718. https://doi.org/10.1039/C7CP02409F

Liu, Z., Ren, X., Cheng, Y., Zhao, G., & Zhou, Y. (2021). Gelation mechanism of alkali induced heat-set konjac glucomannan gel. *Trends in Food Science & Technology, 116*(7), 244–254. https://doi.org/10.1016/j.tifs.2021.07.025

Ozbas, B., Kretsinger, J., Rajagopal, K., Schneider, J. P., & Pochan, D. J. (2004). Salt-triggered peptide folding and consequent self-assembly into hydrogels with tunable modulus. *Macromolecules, 548*(19), 7331–7337. https://doi.org/10.1021/ma0491762

Panja, S., Dietrich, B., Trabold, A., Zydel, A., Qadir, A., & Adams, D. J. (2021). Varying the hydrophobic spacer to influence multicomponent gelation. *Chemical Communications, 57*(64), 7898–7901. https://doi.org/10.1039/d1cc02786g

Patel, A. R., Dumlu, P., Vermeir, L., Lewille, B., Lesaffer, A., & Dewettinck, K. (2015). Rheological characterization of gel-in-oil-in-gel type structured emulsions. *Food Hydrocolloids, 46*, 84–92. https://doi.org/10.1016/j.foodhyd.2014.12.029

Qiao, D., Lu, J., Shi, W., Li, H., Zhang, L., Jiang, F., & Zhang, B. (2022). Deacetylation enhances the properties of konjac glucomannan/agar composites. *Food Hydrocolloids, 276*, Article 118776. https://doi.org/10.1016/j.carbpol.2021.118776

Rafe, A., & Razavi, S. M. A. (2013). Dynamic viscoelastic study on the gelation of basil seed gum. *International Journal of Food Science & Technology, 48*(3), 556–563. https://doi.org/10.1111/j.1365-2621.2012.03221.x

Shilova, O. A. (2020). Fractals, morphogenesis and triply periodic minimal surfaces in sol–gel-derived thin films. *Journal of Sol-Gel Science and Technology, 95*, 599–608. https://doi.org/10.1007/s10971-020-05279-y

Shitrit, Y., & Bianco-Peled, H. (2021). Insights into the formation mechanisms and properties of pectin hydrogel physically cross-linked with chitosan nanogels. *Carbohydrate Polymers, 269*, Article 118274. https://doi.org/10.1016/j.carbpol.2021.118274

Singhal, A., Toth, L. M., Beaucage, G., Lin, J. S., & Peterson, J. (1997). Growth and structure of zirconium hydrous polymers in aqueous solutions. *Journal of Colloid and Interface Science, 194*(2), 470–481. https://doi.org/10.1006/jcis.1997.5117

Solo-de-Zaldívar, B., Tovar, C. A., Borderías, A. J., & Herranz, B. (2014). Effect of deacetylation on the glucomannan gelation process for making restructured seafood products. *Food Hydrocolloids, 35*, 59–68. https://doi.org/10.1016/j.foodhyd.2013.04.009

Tkalec, G., Knez, Ž., & Novak, Z. (2015). Formation of polysaccharide aerogels in ethanol. *RSC Advances, 5*(94), 77362–77371. https://doi.org/10.1039/C5RA14140K

Tong, C., Liu, L., Lin, Q., Liu, J., Xue, Q., Wu, C., & Pang, J. (2022). Insights into the formation of konjac glucomannan gel induced by ethanol equilibration. *Food Hydrocolloids, 126*, Article 107469. https://doi.org/10.1016/j.foodhyd.2021.107469

Tripathi, A., Parsons, G. N., Khan, S. A., & Rojas, O. J. (2018). Synthesis of organic aerogels with tailorable morphology and strength by controlled solvent swelling following hansen solubility. *Scientific Reports, 8*(1), 2106. https://doi.org/10.1038/s41598-018-19720-4

Wagner, N. J., & Mewis, J. (2021). Theory and applications of colloidal suspension rheology. *Cambridge University Press*. https://doi.org/10.1017/9781108394826

Wang, C. F., Ejeta, D. D., Wu, J. Y., Kuo, S. W., Lin, C. H., & Lai, J. Y. (2020). Tuning the Wettability and Surface Free Energy of Poly (vinylphenol) Thin Films by Modulating Hydrogen-Bonding Interactions. *Polymers, 12*(3), 523. https://doi.org/10.3390/polym12030523

Wang, H., Liu, Y., Ling, C., Li, X., Wang, J., & Xie, F. (2018). Insights into the multi-scale structure and digestibility of heat-moisture treated rice starch. *Food Chemistry, 242*, 323–329. https://doi.org/10.1016/j.foodchem.2017.09.014

Wang, J., Liu, B., Ru, G., Bai, J., & Feng, J. (2016). Effect of urea on phase transition of poly(N-isopropylacrylamide) and poly(N, N-diethylacrylamide) hydrogels: A clue for urea-induced denaturation. *Macromolecules, 49*(1), 234–243. https://doi.org/10.1021/acs.macromol.5b01949

Williams, M. A., Foster, T. J., Martin, D. R., Norton, I. T., Yoshimura, M., & Nishinari, K. (2000). A molecular description of the gelation mechanism of konjac mannan. *Biomacromolecules, 1*(3), 440–450. https://doi.org/10.1021/bm005525y

Wu, C. J., Gaharwar, A. K., Chan, B. K., & Schmidt, G. (2011). Mechanically tough pluronic F127/laponite nanocomposite hydrogels from covalently and physically cross-linked networks. *Macromolecules, 44*(20), 8215–8224. https://doi.org/10.1021/ma200562k

Wu, C., Peng, S., Wen, C., Wang, X., Fan, L., Deng, R., & Pang, J. (2012). Structural characterization and properties of konjac glucomannan/curdlan blend films. *Carbohydrate Polymers, 89*(2), 497–503. https://doi.org/10.1016/j.carbpol.2012.03.034

Ye, X., Kennedy, J. F., Li, B., & Xie, B. J. (2006). Condensed state structure and biocompatibility of the konjac glucomannan/chitosan blend films. *Carbohydrate Polymers, 64*(4), 532–538. https://doi.org/10.1016/j.carbpol.2005.11.005

Zhang, Y., Song, Q., Tian, Y., Zhao, G., & Zhou, Y. (2022). Insights into biomacromolecule-based alcogels: A review on their synthesis, characteristics and applications. *Food Hydrocolloids, 128*, Article 107574. https://doi.org/10.1016/j.foodhyd.2022.107574

Zhou, Y., Jiang, R., Perkins, W. S., & Cheng, Y. (2018). Morphology evolution and gelation mechanism of alkali induced konjac glucomannan hydrogel. *Food Chemistry, 269*, 80–88. https://doi.org/10.1016/j.foodchem.2018.05.116

Zhou, Y., Wu, L., Tian, Y., Li, R., & Cheng, Y. (2020). A novel low-alkali konjac gel induced by ethanol to modulate sodium release. *Food Hydrocolloids, 103*, Article 105653. https://doi.org/10.1016/j.foodhyd.2020.105653